Author Manuscript

Author Manuscript

Author Manuscript

Author Manuscript

HHS Public Access

Author manuscript

Neurobiol Dis. Author manuscript; available in PMC 2023 March 01.

Published in final edited form as:

Neurobiol Dis. 2023 March ; 178: 106013. doi:10.1016/j.nbd.2023.106013.

Role of NKCC1 and KCC2 during hypoxia-induced neuronal swelling in the neonatal neocortex

Yusuke Takezawa[a,b], **Rachel Langton**[a,b], **Samuel M. Baule**[c], **Miriam Bridget Zimmerman**[d], **Stephen Baek**[e], **Joseph Glykys**[a,b,f,*]

[a]Dept. of Pediatrics, The University of Iowa, Iowa City, Iowa, USA

[b]Iowa Neuroscience Institute, The University of Iowa, Iowa City, Iowa, USA

[c]Dept. of Biomedical Engineering, The University of Iowa, Iowa City, Iowa, USA

[d]Dept. of Biostatistics, The University of Iowa, Iowa City, Iowa, USA

[e]School of Data Science, University of Virginia, Charlottesville, Virginia, USA

[f]Dept. of Neurology, The University of Iowa, Iowa City, Iowa, USA

Abstract

Neonatal hypoxia causes cytotoxic neuronal swelling by the entry of ions and water. Multiple water pathways have been implicated in neurons because these cells lack water channels, and their membrane has a low water permeability. NKCC1 and KCC2 are cation-chloride cotransporters (CCCs) involved in water movement in various cell types. However, the role of CCCs in water movement in neonatal neurons during hypoxia is unknown. We studied the effects of modulating CCCs pharmacologically on neuronal swelling in the neocortex (layer IV/V) of neonatal mice (post-natal day 8–13) during prolonged and brief hypoxia. We used acute brain slices from Clomeleon mice which express a ratiometric fluorophore sensitive to Cl^- and exposed them to oxygen-glucose deprivation (OGD) while imaging neuronal size and $[Cl^-]_i$ by multiphoton microscopy. Neurons were identified using a convolutional neural network algorithm, and changes in the somatic area and $[Cl^-]_i$ were evaluated using a linear mixed model for repeated measures. We found that (1) neuronal swelling and Cl^- accumulation began after OGD, worsened during 20 min of OGD, or returned to baseline during reoxygenation if the exposure to OGD was brief (10 min). (2) Neuronal swelling did not occur when the extracellular Cl^- concentration was low. (3) Enhancing KCC2 activity did not alter OGD-induced neuronal swelling but prevented Cl^- accumulation; (4) blocking KCC2 led to an increase in Cl^- accumulation during prolonged OGD

This is an open access article under the CC BY-NC-ND license (http://creativecommons.org/licenses/by-nc-nd/4.0/).

*Corresponding author at: Division of Child Neurology, Stead Family Department of Pediatrics, Carver College of Medicine, University of Iowa, 169 Newton Rd, PBDB 2324, Iowa City, IA 52242, USA. joseph-glykys@uiowa.edu (J. Glykys).

Author contributions

JG and YT conceived and designed the study. SB and JG designed the convolutional neural network. YT performed the experiments. YT, SMB, and RL analyzed the data. BZ and YT performed statistical analyses. YT and JG drafted the manuscript and figures. All authors critically evaluated the manuscript and approved the final version of the manuscript.

Declaration of Competing Interest

The authors declare that they have no known competing financial interests or personal relationships that could have appeared to influence the work reported in this paper.

Appendix A. Supplementary data

Supplementary data to this article can be found online at https://doi.org/10.1016/j.nbd.2023.106013.

Author Manuscript Author Manuscript Author Manuscript Author Manuscript

and aggravated neuronal swelling during reoxygenation; (5) blocking NKCC1 reduced neuronal swelling during early but not prolonged OGD and aggravated Cl^- accumulation during prolonged OGD; and (6) treatment with the “broad” CCC blocker furosemide reduced both swelling and Cl^- accumulation during prolonged and brief OGD, whereas simultaneous NKCC1 and KCC2 inhibition using specific pharmacological blockers aggravated neuronal swelling during prolonged OGD. We conclude that CCCs, and other non-CCCs, contribute to water movement in neocortical neurons during OGD in the neonatal period.

Keywords

OGD; Furosemide; Bumetanide; Cytotoxic edema; Neuron; Neonatal

1. Introduction

Perinatal asphyxia leads to poor oxygen perfusion, which can result in hypoxic-ischemic encephalopathy (HIE). HIE, with an overall incidence of 1–2 in every 1000 live births, can cause lifelong neurological sequelae such as cerebral palsy, mental retardation, cerebral visual impairment, deafness, epilepsy, and developmental disabilities (Saw et al., 2019). Although therapeutic hypothermia is the standard treatment for HIE, as it reduces mortality, disability, and seizures (Azzopardi et al., 2014; Gluckman et al., 2005; Orbach et al., 2014), there is no pharmacological treatment available to prevent brain swelling. Current treatments for brain edema, evaluated in adults, using mannitol, hypertonic saline, and craniectomy are woefully inadequate, resulting in significant mortality and disability (Cooper et al., 2011; Hutchinson et al., 2016; Kolias et al., 2022). Thus, it is critical to understand how neonatal hypoxic brain injury causes neuronal swelling and altered ionic homeostasis, as they can lead to neuronal cell death and increased seizures (Blauwblomme et al., 2018; Sekhon et al., 2017).

Studies in juvenile and adult brain slices have shown that hypoxia induces astrocytic and neuronal swelling (Hellas and Andrew, 2021; Meyer et al., 2021; Risher et al., 2009). Neuronal cytotoxic edema results from an influx of ions, primarily Na^+ and Cl^-, accompanied by water, from the interstitial space into the intracellular compartment (Glykys et al., 2017; Halstead and Geocadin, 2019). Neurons do not have functional water channels (aquaporins), and their membranes have a low water permeability (Andrew et al., 2007; Fettiplace and Haydon, 1980; Tong et al., 2012). Thus, various pathways have been proposed to account for water movement in neurons in association with ionic shifts, especially Cl^- (Glykys et al., 2017; Hoffmann et al., 2009; Zeuthen, 2010), as this anion is essential for cytotoxic edema (Rungta et al., 2015; Steffensen et al., 2015; Weilinger et al., 2022). Among them, the cation-chloride cotransporters (CCCs) NKCC1 and KCC2 are membrane proteins involved in the movement of cations and Cl^-(Kahle et al., 2015; Portioli et al., 2021). They have been implicated in restoring the $[Cl^-]_i$ set point in neurons (Delpire and Staley, 2014; Glykys et al., 2014; Rahmati et al., 2021; Weilinger et al., 2022) but also see (Doyon et al., 2016; Dusterwald et al., 2018). Also, these CCCs cotransport water with the ions in non-neuronal cells (Hamann et al., 2010; Steffensen et al., 2018; Zeuthen, 2010;

Author Manuscript Author Manuscript Author Manuscript Author Manuscript

Zeuthen and Macaulay, 2012; Zhang et al., 2021), yet whether they are water-pumps is still an area of intense study (Portioli et al., 2021; Zhang et al., 2021).

The participation of CCCs in neuronal water movement is unclear. Several studies have demonstrated that blocking the Na^+-K^+-Cl^- cotransporter (NKCC1) reduces cerebral edema and infarct size in mice (Chen et al., 2005; Wang et al., 2014; Yan et al., 2003; Yan et al., 2001). However, this could reflect a reduction in astrocytic rather than neuronal swelling. Blocking NKCC1 did not decrease neuronal swelling during NMDA excitotoxic injury (Rungta et al., 2015), yet it reduced neuronal swelling induced by controlled cortical impact (Sawant-Pokam et al., 2020). Importantly, it is unclear if CCCs are involved in hypoxia-induced neuronal swelling during the neonatal period when NKCC1 expression is high (Dzhala et al., 2005; Plotkin et al., 1997; Wang et al., 2002). Here, we evaluated neuronal swelling and the changes in $[Cl^-]_i$ during oxygen-glucose deprivation (OGD) in acute brain slices during the early neonatal period (post-natal day 8–13) and the contribution of NKCC1 and KCC2 to neuronal swelling using pharmacological manipulations.

2. Material and methods

2.1. Mice and preparation of acute brain slices

Neuronal area and $[Cl^-]_i$ were measured in brain slices from post-natal (P8–13) CLM-1 Clomeleon mice (a gift from Kevin J. Staley and obtained from JaxLab (B6.Cg-Tg(Thy1-Clomeleon)1Gjau/J)) which robustly express the Cl^- sensitive fluorophore in neocortical layer IV/V pyramidal neurons. Mice of both sexes were anesthetized with inhaled isoflurane and decapitated per a protocol approved by the Institutional Animal Care and Use Committee of the University of Iowa. The brain was removed and placed in ice-cold artificial cerebrospinal fluid (aCSF) containing (in mM) NaCl (120), KCl (3.3), $CaCl_2$ (1.3), $MgCl_2$ (2), NaH_2PO_4 (1.25), $NaHCO_3$ (25), and D-glucose (10) with pH 7.3–7.4 when bubbled with carbogen (95% O_2 and 5% CO_2). Coronal brain slices 450 μm thick were cut using a vibratome (Leica VT1000S) while submerged in aCSF containing 2 mM kynurenic acid to block glutamatergic receptors. The brain slices were placed in an interface holding chamber containing aCSF (1.3 mM $MgCl_2$) at room temperature for 30 min, after which the temperature was slowly increased to and maintained at 30 °C. Slices were stored for at least 1-h before being transferred to the recording chamber.

2.2. Optical imaging

The area and $[Cl^-]_i$ of the neocortical neurons (layer IV/V, motor, and somatosensory regions) were imaged using a two-photon microscope. A Bruker Ultima In Vitro galvo-resonant system was mounted on an Olympus BX51WIF upright microscope with a 20× water immersion objective (NA 1.00). A Ti: sapphire mode-locked laser (Mai Tai HPDS; Spectra-Physics) generated two-photon excitation at 860 nm. Emitted light was bandpass filtered at 510 nm (T510lpxrxt, Chroma) and then at 480/40 nm for cyan fluorescence protein (CFP) and 535/30 nm for yellow fluorescence protein (YFP). Two GaAsPs or multi-alkali photomultiplier tubes (Hamamatsu Photonics) were used to acquire CFP and YFP signals simultaneously. Three-dimensional stacks (3D) of raster scans in the XY plane were imaged at 2 μM intervals with a 512 × 512-pixel resolution.

Author Manuscript Author Manuscript Author Manuscript Author Manuscript

2.3. OGD experiments

The OGD solution consisted of regular aCSF where D-glucose was replaced with D-mannitol (10 mM), and the O_2 in the carbogen mixture was replaced with 95% N_2 while 5% CO_2 was maintained. Before OGD was induced, a baseline image was taken in aCSF (oxygenated). Slices were then perfused with regular aCSF or a drug, and another image was taken 5–10 min after (Time 0 min) before exposing them to brief OGD (10 min), followed by oxygenated aCSF (15 min, washout) or further OGD (10 additional min, prolonged). The slices were imaged at several time points. For the low extracellular Cl^- experiments, the Cl^- in the aCSF and OGD solutions was replaced with gluconate to keep osmolality and other components the same [Na-gluconate (120), K-gluconate (3.3), Ca-gluconate (1.3), Mg-gluconate (1.3), NaH_2PO_4 (1.25), $NaHCO_3$ (25), and D-glucose (10)]. All experiments were performed at 30–32 °C.

2.4. Measurement of neuronal somatic area and $[Cl^-]_i$

Neuronal somas in the fluorescent images (region of interest, ROI) were detected using an automated neuronal morphology analysis framework (ANMAF) based on masked region convolutional neuronal networks (mask R-CNN) that we had developed previously (Tong et al., 2021). This allowed human-free selection of the neuronal area, avoiding bias. Briefly, the CFP and YFP z-stack images were loaded, and the corresponding background signal was subtracted from the entire 3D stack. Next, 3D planes were median filtered, and maximum intensity *Z*-projections were created every 10 μM for neuronal area determination. Thus, each neuron's maximal area (MaxArea, YFP signal) projection was in a single-plane (Glykys et al., 2019). The drawing of the ROIs around the cell bodies was automated (by ANMAF) on the YFP channel, and the ROI area and YFP/CFP calculations were done with ImageJ (National Institutes of Health). The YFP/CFP fluorescence ratio was calculated for each pixel in the ROI at the z-plane corresponding to the MaxArea. Next, the median YFP/CFP ratio for the entire ROI was calculated. The photomultiplier tube sensitivity was evaluated routinely, and if it deviated, the ratio was corrected offline using a linear (GaAsPs) or non-linear (multi-alkalis) regression model. The YFP/CFP ratio was converted to $[Cl^-]$ using the following equation:

$$[Cl^-]_i = K'_D \frac{(R_{max} - R)}{(R - R_{min})}$$

Where K'_D is the apparent dissociation constant, R_{max} is the ratio when Clomeleon is not bound to Cl^-, and R_{min} is the ratio when Clomeleon is completely quenched. The K'_D, R_{max}, and R_{min} were determined using solutions of different Cl^- concentrations as previously described (Glykys et al., 2009). The following values were obtained: K'_D of 106.5 mM, R_{max} of 0.921, R_{min} of 0.238 for the GaAsPs, and K'_D of 111.6 mM, R_{max} 1.438, and R_{min} 0.367 for the multi-alkali photomultipliers (Supp. Fig. 1). The values are similar to those published previously (Duebel et al., 2006; Glykys et al., 2014). Only neurons with $[Cl^-]_i$ at baseline above 200 mM were excluded from all analyses (1.44%) as they most likely represented injured or dying neurons. Neurons with YFP/CFP conversion to $[Cl^-]_i$ that resulted in negative values (YFP/CFP higher than Rmax, 17.3% of neurons; −6.8 mM [−7.3, −6.3] median ± 95%CI) were considered to have a $[Cl^-]_i$ of 1 mM (for

Author Manuscript Author Manuscript Author Manuscript Author Manuscript

fold-change calculations) and included for the analysis for MaxArea, YFP/CFP, and $[Cl^-]_i$. In the results sections, we describe the YFP/CFP ratio fold-change of all included neurons, which is independent of calibration, showing similar fold changes as $[Cl^-]_i$. Neurons (ROIs) that could be followed at all time points during an experiment were used for the analysis. The ROIs at different time points were matched using a custom-made macro under IgorPro (Wavemetrics).

2.5. Reagents

D-glucose, mannitol, kynurenic acid, bumetanide, VU0463271 (VU), CLP257, and furosemide were obtained from Sigma-Aldrich (St. Louis, MO). Bumetanide was diluted from an ethanol stock solution to a final concentration of 10 μM (0.02% Ethanol). VU0463271 was diluted from a DMSO stock solution to a final concentration of 10 μM (0.2% DMSO). CLP257 was dissolved in DMSO before addition to the experimental solutions at a final concentration of 10 μM (0.1% DMSO). Furosemide was dissolved in DMSO at a final concentration of 300 μM (0.1% DMSO). All stock solutions were used within a week of preparation.

2.6. Statistical analysis

MaxArea, and its change over time, are expressed as mean ± 95% confidence interval (95% CI). $[Cl^-]_i$ and YFP/CFP are expressed as a geometric mean ± 95% CI, as $[Cl^-]_i$ follows a log-normal distribution. A linear mixed model for repeated measures was used to estimate and test for the significance of the mean change in MaxArea, the YFP/CFP ratio, and the $[Cl^-]_i$ relative to baseline at each time point (control-5′ or drug-10′, OGD-5′, 10′, 15′, and 20′) and for each treatment group. As the YFP/CFP ratio and $[Cl^-]_i$ have a right-skewed distribution, we used the natural log transformation of the data in our statistical analyses. A linear mixed model for repeated measures was also used for each outcome measure using change from baseline as the dependent variable, treatment group, phase, and group*phase interaction as the fixed effects, and baseline measure as a covariate. Since the data for these experiments were obtained from repeated measurements in cells within tissue slices from animals in each treatment group, the mixed model also accounted for the variation caused by these random effects and the covariance structure that best fit the repeated measures from the neurons within each tissue slice was identified. From this fitted model, pairwise group means comparisons were made for each drug and no-drug group at OGD-10′ and OGD-20′ using Dunnett's test and applying *p*-value adjustment for the two phases tested. A similar analysis was performed for the brief OGD experiments, with drug versus no-drug comparisons at OGD-10′ and washout-15′. For groups with more than one mouse for each sex, the sample size is small for statistical testing of sex differences as the study was not powered to detect for this aim. Thus, instead of providing *p*-values, an estimate (with 95% CI) of the mean difference between males and females is presented in Supp. Table. 1.

A binary outcome, defined as a meaningful change from the baseline, was used as the criterion to classify the direction of change in MaxArea. For this analysis, the magnitude of a significant change was first determined using data from aCSF experiments of the repeated measurements of neuronal areas. We fitted a random effects model with mice, tissue slice within mice, and neuron within slice within mice as random effects to estimate variance

Author Manuscript Author Manuscript Author Manuscript Author Manuscript

components for the variations between mice, between slices within mice, between neurons within tissue within mice, and variation between repeated measures within a neuron. The variation between repeated measures within a neuron was used to compute the standard deviation (SD) of the difference in MaxArea between repeated measures. A meaningful change was defined as a change >1 SD of the difference. Using this definition, a change in MaxArea from baseline at OGD-10′ and OGD-20′ was categorized as a meaningful change. The number of neurons with a meaningful change relative to the total number of neurons in a tissue slice was used as the outcome in a generalized linear mixed model with a logit link. The treatment group and phase were used as the dependent variables to estimate the mean proportion of neurons that underwent a meaningful change in MaxArea for each drug and to compare them to no-drug conditions. Dunnett's test was used when comparing the six drugs to the no-drug condition, and additional p-value adjustments were applied for the two phases tested. A similar analysis was performed for the brief OGD experiments. To assess the linear association between a change from baseline in neuronal MaxArea and $[Cl^-]_i$ at OGD-10′, OGD-20′, and washout-15′, a random coefficient regression was used to estimate the mean intercept and mean slope. Statistical significance was set at $p < 0.05$. GraphPad Prism (v.9.0.1; GraphPad Software) and SAS 9.4 (SAS/STAT 15.2; SAS Institute Inc.) were used for data analysis.

3. Results

3.1. Prolonged hypoxia causes neuronal swelling and raises $[Cl^-]_i$ in the neonatal neocortex

We first analyzed the effect of prolonged OGD (20 min) on neuronal body size (neocortex layer IV/V) in acute brain slices prepared from neonatal Clomeleon mice (P8–13). We measured the neuronal somatic area (MaxArea, YFP signal) using a convolutional neural network to avoid a human bias (Tong et al., 2021). We matched 247 neurons that were identifiable at all time points (10 slices, 3 mice). Neuronal MaxArea did not change between 0 and 5 min in oxygenated aCSF. However, it increased significantly from baseline (257 μm^2 [203,312]; mean [95% CI]) by 5 min of OGD and increased further by 20 min of OGD (mean difference OGD-20′: 32.3 μm^2 [25.2, 39.4], $p < 0.0001$, linear mixed model; Fig. 1A, B). The swelling was independent of the initial size of the neurons at OGD-20′ (Fig. 1C).

We next determined the proportion of neurons whose areas increased, decreased, or did not change during prolonged OGD using a size threshold of 19.3 μm^2 [18.6, 20.1]. This value is the standard deviation from any two repeated MaxArea measurements when neurons were perfused with aCSF for 20 min (see below). Under OGD, the proportion of neurons that swelled increased to 38.5% [30.6, 47.0] by 10 min (OGD-10′) and to 58.7% [50.1, 66.8] by 20 min (OGD-20′, Fig. 1D). For these and the following experiments, these time points were chosen as there was an apparent change in MaxArea compared to baseline (Fig. 1B).

Prolonged OGD also led to a significant increase in the neuronal $[Cl^-]_i$. By OGD 10′, the proportional increase in neuronal $[Cl^-]_i$ was 2.96-fold [2.27, 3.87] from a baseline of 30.4 mM [24.3, 38.1] (geometric mean [95% CI]), and by OGD-20′ it had increased by 4.21-fold [3.29, 5.40] ($p < 0.0001$; Fig. 1E). The YFP/CFP ratio, which is independent of Cl^- calibration, also decreased significantly ($p < 0.0001$; Fig. 1E). There was a significant

Author Manuscript Author Manuscript Author Manuscript Author Manuscript

positive correlation between the change in MaxArea and $[Cl^-]_i$ at OGD-10′, but not at OGD-20′ (Supp. Fig. 2). This suggest that both water and $[Cl^-]_i$ accumulate during early OGD (10 min) and reach a plateau by 20 min. During control conditions, in the absence of OGD, neurons did not swell over 20 min, and the $[Cl^-]_i$ decreased slightly (Supp. Fig. 3). These results indicate that during the neonatal period, neocortical neurons progressively swell and accumulate $[Cl^-]_i$ early during hypoxia.

3.2. Brief hypoxia causes reversible neuronal swelling and Cl^- accumulation in the neonatal neocortex

In clinical settings, especially during neonatal hypoxia, most patients are resuscitated and recover from acute hypoxia (Heathcote et al., 2018). Thus, we tested the effect of a short exposure to OGD (Brief OGD) on neuronal size. A 10-min OGD perfusion (Obeidat et al., 2000; Povysheva et al., 2019) was followed by a 15-min washout with carbogen aCSF (washout-15′, Fig. 1F). We matched 425 neurons (10 slices, 3 mice). OGD for 10 min led to a 15.6 μm^2 [9.36, 21.8] increase in neuronal MaxArea, from a baseline of 245 μm^2 [216, 274] ($p < 0.0001$). The neuronal size returned to baseline 15 min after washout and was just 2.59 μm^2 [−4.09, 9.27] above baseline (Fig. 1G). The proportion of neurons that swelled >1 SD from their baseline was highest at OGD-10′ (44% [37.5, 50.7]) and decreased steadily during washout (Fig. 1H). Interestingly, by 15 min of washout, 30.6% [24.8, 37.1] of neurons remained swollen, and 24% [18.8, 30.2] had decreased in size. In other words, even after 15 min of washout with oxygenated aCSF and the return of the average neuronal MaxArea to baseline, a proportion of them remained swollen. These changes in neuronal MaxArea mirrored the shift in neuronal YFP/CFP and $[Cl^-]$. The $[Cl^-]_i$ increased by 2.27-fold [1.55, 3.35] from a baseline of 24.9 mM [18.8, 33.0]; $p < 0.0001$) at OGD-10′ and returned to baseline by 15 min (Fig. 1I, J). The relationship between change in MaxArea and $[Cl^-]_i$ after 15-min of washout was negative but non-significant (Supp. Fig. 2). Collectively, these results show that neonatal neocortical neurons exposed to brief hypoxia (10 min) swell and accumulate Cl^- but can return to baseline during re-oxygenation.

3.3. OGD-mediated neuronal swelling requires Cl^- entry

Previous studies in juvenile and adult rodents showed that Cl^- entry is required for neuronal and dendritic swelling (Rungta et al., 2015; Steffensen et al., 2015; Weilinger et al., 2022). Whether this is also the case in neonatal neurons during OGD is unclear. Also, the measurement of $[Cl^-]_i$ during OGD may be overestimated because Clomeleon is sensitive to pH changes when the $[Cl^-]_i$ is high (>50 mM) (Kuner and Augustine, 2000), and hypoxia leads to a small decrease in intracellular pH (0.14 units) (Pond et al., 2006). Thus, we evaluated the contribution of extracellular Cl^- concentration to neuronal swelling and the change of $[Cl^-]_i$ during OGD.

During recordings in oxygenated aCSF with low extracellular Cl^-(Low-Cl^-), neuronal MaxArea decreased, and $[Cl^-]_i$ increased ($n = 251$ matched neurons, 4 slices, 3 mice; Supp. Fig. 4). Similar outcomes were observed during OGD recordings in Low-Cl^- aCSF ($n = 208$ neurons, 5 slices, 3 mice; Supp. Fig. 4). Importantly, there was no significant difference in neuronal size and proportional $[Cl^-]_i$ change between aCSF and OGD experiments with Low-Cl^-($p = 0.25$ and higher). These results indicate that neuronal swelling under

Author Manuscript Author Manuscript Author Manuscript Author Manuscript

OGD requires Cl^- entry. Also, the lack of YFP/CFP and $[Cl^-]_i$ difference between OGD and aCSF in Low-Cl^- suggests that an OGD-induced change in intracellular pH does not significantly alter Clomeleon measurement as one would have expected a higher $[Cl^-]_i$ in low-Cl^- conditions between OGD vs. oxygenated aCSF.

3.4. Enhancing KCC2 activity does not prevent neuronal swelling but avoids Cl^- accumulation

CCCs are involved in water movement in different cells (Hamann et al., 2010; Steffensen et al., 2018; Zeuthen, 1994; Zeuthen, 2010; Zeuthen and Macaulay, 2012). Yet, whether CCCs play such a role in neocortical neurons during early brain development when both KCC2 and NKCC1 are expressed is unclear. We first hypothesized that if KCC2 primarily participates in water extrusion, enhancing its activity should reduce the accumulation of water and Cl^-. We conducted OGD experiments, both prolonged and brief, while enhancing KCC2 activity with CLP257 (10 μM) (Dzhala and Staley, 2021; Gagnon et al., 2013).

During prolonged OGD, neuronal swelling occurred even in CLP257 (n = 346 matched cells, 6 slices, 3 mice; Fig. 2A, B). The neuronal MaxArea increased by 17 μm^2 [6.08, 27.9] after 10 min of OGD, with 32.7% [26.3, 39.7] of neurons swelling. By OGD-20′, the neuronal MaxArea rose by 44.7 μm^2 [33.1, 56.3] with 69.9% [63, 76.1] of neurons swelling (Fig. 2C). When the neuronal MaxAreas during CLP257 were compared to those for no-drug, the means did not differ significantly at OGD-10′ or OGD-20′ ($p > 0.99$ and $p = 0.132$ respectively) yet the mean change was negative at OGD-10′ (–0.37 μm^2 difference [–12.9, 12.1]; Fig. 5A). Also, the proportion of swollen neurons at these time-points was the same for CLP257 and no drug (Fig. 5B).

Whereas CLP257 did not reduce the amount of neuronal swelling, it prevented the accumulation of neuronal Cl^- during OGD with a significant decrease at 5 and 10 min compared to the baseline (0.48-fold-decrease [0.33, 0.69], $p < 0.0001$ and 0.55 [0.38, 0.80], $p < 0.01$, respectively). However, CLP257 did not prevent an increase at OGD-20′ (4.59-fold increase [3.18, 6.63]; Fig. 2D, E). Compared to no-drug, CLP257 caused a lower proportional change in $[Cl^-]_i$ at OGD-10′ but not at OGD-20′ (Fig. 5A).

CLP257 did not prevent neuronal swelling during brief OGD, which was maximal at OGD-10′ ($p < 0.001$) with 35.2% [29.5, 41.3] of neurons swelling followed by a return to baseline during washout (495 neurons, 6 slices, 3 mice; Fig. 2F–H). This degree of neuronal swelling was smaller than observed during no-drug OGD perfusion but was not significant (–3.80 μm^2 difference [–12.9, 5.26] $p > 0.99$; Fig. 5C). CLP257 prevented the proportional increase in $[Cl^-]_i$ from baseline with a significant reduction after 15 min of washout (0.49-fold-decrease [0.35, 0.69], $p < 0.0001$; Fig. 2I, J). The effect of CLP257 on $[Cl^-]$ was significantly different compared to no-drug at OGD-10′ and washout-15′ (Fig. 5C).

In summary, enhancing KCC2 activity with CLP257 prevented Cl^- accumulation. On the other hand, although neuronal swelling was slightly less at OGD-10′ in the presence of CLP257 than in its absence, the difference was not statistically significant. To further test the role of KCC2 in water movement, we decided to block its activity.

Author Manuscript Author Manuscript Author Manuscript Author Manuscript

3.5. Blocking KCC2 exacerbates neuronal swelling during washout and increases Cl^- accumulation during prolonged OGD

We blocked KCC2 with its antagonist VU0463271 (10 μM) and evaluated its effect on neuronal swelling and $[Cl^-]_i$ during OGD. During prolonged OGD, from a baseline of 251 μm^2 [228, 274], neurons started swelling as early as OGD-5′ (8.37 μm^2 increase [4.31, 12.4]; $p < 0.0001$). They swelled further over time and were 36.3 μm^2 [29.5, 43.0] larger by OGD-20′ ($p < 0.0001$; $n = 389$ neurons, 8 slices, 4 mice; Fig. 2B). Compared to no-drug condition, blocking KCC2 did not significantly change neuronal MaxArea (p > 0.99, Fig. 5A) or the proportion of neurons that swelled (Fig. 5B). Blocking KCC2 progressive increased $[Cl^-]_i$ at OGD-10′, –15′ and –20′ compared to the baseline (1.57-fold [1.15, 2.16], $p < 0.01$; 6.84-fold [5.17, 9.05], $p < 0.0001$; and 8.51-fold [6.41, 11.3], $p < 0.0001$; respectively, Fig. 2D, E). The proportional change in $[Cl^-]$ was lower at OGD-10′ with the drug than without, yet still accumulating, and higher at OGD-20′ ($p < 0.0001$, and $p = 0.001$, Fig. 5A).

Similarly, during brief OGD, blocking KCC2 with VU0463271 did not prevent neuronal swelling, which started with drug perfusion (339 neurons, 8 slices, 4 mice). Importantly, swollen neurons did not return to baseline by washout-15′ and remained 19.7 μm^2 [13.6, 25.8] above baseline ($p < 0.0001$; Fig. 2G). Neuronal MaxArea did not differ from the no-drug condition at OGD-10′ but was larger in the VU group after washout-15′ (mean difference 17.2 μm^2 [8.08, 26.4], $p < 0.0001$; Fig. 5C). Also, at washout-15′, there was a larger proportion of swollen neurons ($p < 0.001$) and a smaller proportion of neurons that had shrunk ($p < 0.01$; Fig. 5D). At OGD-10′, the $[Cl^-]_i$ increased by 1.93-fold [1.07, 3.48] ($p < 0.05$), as during prolonged OGD, which returned to baseline at washout-10′ (Fig. 2I, J). The difference in the fold change in $[Cl^-]_i$ between VU treatment and no-drug was not significant ($p > 0.99$; Fig. 5C).

These data, in conjunction with those for CLP257, suggest that KCC2 is involved in some water extrusion, especially during reperfusion. Also, KCC2 was important for the extrusion of Cl^- during prolonged OGD, as blocking this transporter worsened Cl^- accumulation. As there was no further Cl^- accumulation during reperfusion, our data suggest that other transporters or channels can extrude Cl^- from neurons to compensate for the lack of outward KCC2 pumping activity when this transporter is blocked.

3.6. Blocking NKCC1 decreases neuronal swelling and Cl^- accumulation during early OGD

NKCC1 has been associated with the cotransport of water in various cell types (Hamann et al., 2010; Steffensen et al., 2018; Su et al., 2002; Zeuthen and Macaulay, 2012). We evaluated its role in neuronal swelling during OGD during early brain development, a time at which its expression is high (Dzhala et al., 2005; Plotkin et al., 1997). We hypothesized that the NKCC1 blocker bumetanide (10 μM) would reduce the entry of water and Cl^- during OGD, preventing neuronal swelling and Cl^- accumulation.

During prolonged OGD, in the presence of bumetanide, neuronal swelling and Cl^- accumulation were delayed starting at OGD-10′, whereas, in the absence of bumetanide, the

Author Manuscript Author Manuscript Author Manuscript Author Manuscript

increase began at OGD-5′ (n = 487 neurons, 18 slices, 6 mice; Fig. 3A–D). At OGD-10′, the neuronal MaxArea was significantly smaller in bumetanide compared to no-drug (mean difference –11.2 μm^2 [–19.3, –2.97], p = 0.002; Fig. 5A**, left**), and fewer neurons swelled (Bum: 24.4% [19.6, 30.0], no-drug: 38.5% [30.6, 47]; p < 0.01; Fig. 5B). The proportional change in $[Cl^-]_i$ was also lower at OGD-10′ in the presence vs. the absence of bumetanide (0.41-fold-less [0.28, 0.58], p < 0.0001; Fig. 5A, **right**). However, bumetanide did not lessen neuronal swelling and worsened Cl^- accumulation at OGD-20′ compared to no-drug (Fig. 5A).

During brief OGD, similar changes in neuronal MaxArea and $[Cl^-]_i$ were observed at OGD-10′, and both returned to baseline at the end of washout (n = 518, 16 slices, 6 mice; Fig. 3E–H). In the presence of bumetanide, neuronal MaxArea was significantly lower at OGD-10′ than under no-drug condition (mean difference −10.8 μm^2 [−18.8, −2.75], p = 0.002), the proportion of swollen neurons was smaller (Bum: 20.1% [15.7, 25.5], no-drug: 44.0% [37.5, 50.7]; p < 0.001), and the proportional change in $[Cl^-]_i$ decreased (0.45-fold decrease [0.26, 0.77], p = 0.0004; Fig. 5C, D). No significant differences were observed between bumetanide and no-drug condition at washout-15′.

In summary, blocking NKCC1 decreased neuronal swelling and Cl^- accumulation during early OGD (10 min). During prolonged OGD (20 min), the swelling was not ameliorated, and Cl^- accumulation worsened. These findings suggest that although blocking NKCC1 may decrease water and Cl^- accumulation early during OGD, this transporter may reverse during prolonged OGD, pumping Cl^- out (Brumback and Staley, 2008).

3.7. Furosemide, but not simultaneous NKCC1 and KCC2 blockade, reduces neuronal swelling and Cl^- accumulation during OGD

Furosemide is a broad-spectrum CCC blocker that prevents Cl^- accumulation during OGD in adult brain slices (Pond et al., 2006), and it reduces the production of CSF by the choroid plexus (Steffensen et al., 2018). We investigated the effects of furosemide (300 μM) on neuronal swelling and $[Cl^-]_i$ in the neonatal neocortex during OGD.

Furosemide had the largest effect on preventing neuronal swelling and Cl^- accumulation. When it was present, neuronal size did not increase during prolonged OGD (maximal change at OGD-20′: 8.63 μm^2 (−0.97, 18.2), p > 0.05; n = 220 neurons, 8 slices, 4 mice), nor did the proportion of swollen neurons (Fig. 4A–C). Neuronal MaxArea was significantly lower than in no-drug at OGD-10′ and –20′ min (mean difference –15.7 μm^2 [−25.8, −5.55], p = 0.0002 and –24.1 μm^2 [−36.3, −11.8], p < 0.0001, respectively; Fig. 5A), as was the proportion of swollen neurons (p < 0.001; Fig. 5B). Although the neuronal $[Cl^-]_i$ increased over baseline at later time points during OGD (15 and 20 min, Fig. 4D, E), the proportional increase in $[Cl^-]_i$ was lower in the presence of furosemide than in its absence at OGD-10′ and –20′ (p <0.0001, Fig. 5A).

During brief OGD in furosemide, neuronal size did not increase over baseline except for a minimal increase at 10 min of washout (n = 233 neurons, 8 slices, 4 mice; Fig. 4F, G). Importantly, it was significantly lower than under the no-drug condition at OGD-10′ (mean difference, −14.6 μm^2 [−22.4, −6.78], p ≤0.0001; Fig. 5C). The proportion of

Author Manuscript Author Manuscript Author Manuscript Author Manuscript

swollen neurons was also lower at OGD-10′ under furosemide than no-drug (Fig. 5D). Consistent with our findings from the prolonged OGD experiments, furosemide prevented Cl^- accumulation at OGD-10′ (Fig. 4I, J), and it was significantly lower than the no-drug condition (Fig. 5C). Thus, a broad CCC blocker prevented neuronal swelling and Cl^- accumulation during prolonged and brief OGD.

Furosemide has been described to block other receptors and transporters, including $GABA_A$Rs, carbonic anhydrase, and the Na^+-independent Cl^-/HCO_3^- exchanger when used in the micromolar range (Halligan et al., 1991; Navon et al., 1975; Wafford et al., 1996). Thus, we set out to determine whether simultaneously blocking NKCC1 and KCC2 with their specific antagonists, bumetanide (10 μM) and VU0463271 (10 μM), reproduces the effects of furosemide. We found that during prolonged OGD, neuronal size MaxArea increased above baseline starting at the time of drug application and continued throughout OGD, rising by 65.3 μm^2 [53.6, 77.0] at OGD-20′ (n = 130 neurons, 6 slices, and 3 mice; $p < 0.0001$; Fig. 4B). At OGD-20′, this swelling was significantly higher than that observed under no-drug condition (mean difference: 33.4 μm^2 [19.9, 47.0], $p < 0.0001$; Fig. 5A). Also, the proportion of swollen neurons at OGD-20′ was significantly higher than under no-drug (84.6% [74.2, 91.3], $p < 0.0001$; Fig. 5B). A proportional increase in the $[Cl^-]_i$ was also observed starting at OGD-10′ (Fig. 4D, E; $p < 0.0001$), yet it did not differ significantly that under the no-drug condition (Fig. 5A).

During brief OGD, bumetanide + VU0463271 caused significant swelling not only at OGD-10′ but even at washout-5′ and 10′ min. Neuronal MaxArea returned to baseline only after 15 min (n = 147, 6 slices, 3 mice; Fig. 4G). This increase was similar to under the no-drug condition at OGD-10′ and washout-15′ ($p > 0.99$; Fig. 5C). A proportional increase in neuronal $[Cl^-]_i$ occurred at OGD-10′ and during washout and only returned to baseline by washout-15′ (Fig. 4J). This effect was similar to no drug condition at OGD-10′ and 15 min of washout ($p > 0.99$; Fig. 5C).

These results show that furosemide prevents neuronal swelling and Cl^- accumulation during prolonged and brief OGD. However, the fact that these effects were not mimicked by simultaneously blocking NKCC1 and KCC2 with their specific antagonist suggests that furosemide prevents the entry of water and Cl^- via additional pathways besides NKCC1 and KCC2.

4. Discussion

In this study, we aimed to measure swelling dynamics in neonatal cortical neurons during prolonged and brief OGD and determined the roles of CCCs in this pathological condition. We found that: 1) prolonged OGD results in persistent neuronal swelling and Cl^- accumulation, whereas brief OGD results in similar changes that can reverse on re-oxygenation; 2) OGD-induced neuronal swelling during the neonatal period depends on the influx of extracellular Cl^-; 3) blocking NKCC1 decreases neuronal swelling and Cl^- accumulation early during OGD; 4) KCC2 modulation alters the movement of neuronal Cl^-, and to a lesser degree water; and 5) furosemide prevents neuronal swelling and Cl^- accumulation during prolonged and brief OGD, but through other pathways in addition to

Author Manuscript Author Manuscript Author Manuscript Author Manuscript

CCCs. Our results suggest that blocking NKCC1 with bumetanide and other water pathways with furosemide could decrease neuronal swelling during perinatal asphyxia.

Several aspects of our methodology enhanced the rigor of our experiments. We used ANMAF to measure neuronal size (YFP signal) to avoid human bias (Tong et al., 2021). Neurons were matched to their baseline rather than population averages as neuronal size and $[Cl^-]_i$ vary from cell to cell and slice to slice. This approach also enabled us to determine the proportion of neurons that swelled. A linear mixed model was used for statistical analysis, nesting cells in slices and thus preventing a single slice from swaying the analysis. Non-swelling neurons were not excluded, providing an accurate picture of the effect of OGD and drugs on a neuronal population. The changes in the proportional YFP/CFP were assessed in addition to $[Cl^-]_i$ whose derivation depends on calibration curves. Thus, these approaches allowed us to increase the rigor of our study.

Our study also had some limitations. First, we used Clomeleon, which has a high Kd, to measure Cl.− We observed variability in baseline $[Cl^-]_{i,}$ between slices and neurons of the same slice. However, our values agree with prior publications, including in vivo data using a different fluorophore (Blauwblomme et al., 2018; Duebel et al., 2006; Ebihara et al., 1995; Glykys et al., 2014; Glykys et al., 2009; Sulis Sato et al., 2017; Kuner and Augustine, 2000). Importantly, we matched neurons and compared them to their own baseline and not the population baseline allowing us to determine fold changes in YFP/CFP (independent of $[Cl^-]_i$ calibration) and Cl^-. Second, Clomeleon is also sensitive to pH changes at high Cl^- values (Cl^- can be overestimated in acidotic pH), and we did not measure pH as it was outside the scope of this study. However, multiple investigators have achieved robust findings using this fluorophore (Berglund et al., 2008; Duebel et al., 2006; Kuner and Augustine, 2000), including during OGD experiments (Blauwblomme et al., 2018; Pond et al., 2006) and our primary interest was the directional change in $[Cl^-]_i$ and not the absolute Cl^- values. An alternative interpretation to the elevated $[Cl^-]_i$ observed in the Low-Cl^- experiments is that it represents elevated pH caused by seizure-like activity (Raimondo et al., 2012; Yamamoto and Kawai, 1968) affecting Clomeleon measurement. However, we do not favor this interpretation as it takes time for the exchange of regular Cl^- with low-Cl^- solution and astrocytes play a role in buffering the $[Cl^-]_o$ (Egawa et al., 2013), so the $[Cl^-]_o$ is unlikely to be zero during our imaging time frame. We imaged multiple slices, so the probability of always landing on a supposed seizure is unlikely. A recent publication using a non-pH sensitive dye (MQAE-FLIM) also showed a small increase in $[Cl^-]_i$ in Low-Cl^- aCSF (Weilinger et al., 2022). Also, using CLP257 and furosemide in our experiments also prevented an increase in $[Cl^-]_i$ during early OGD, arguing against a significant pH effect affecting Clomeleon measurement. Third, we did not use transgenic mice but relayed on pharmacology. However, transgenic mice have their limitations, including compensatory processes that can mask a mechanism of interest, especially regarding neuronal volume regulation in which multiple and redundant pathways participate. Thus, we considered the pharmacologic approach an important early step in this area. CCC expression has shown sex differences during early brain development (Galanopoulou, 2007; Murguia-Castillo et al., 2013). There may be some indications of a sex difference in our results where the 95% CI does not include 0 for MaxArea (e.g. bumetanide data; see Methods and Supp. Table 1), but our study was not powered to detect sex differences and would warrant further investigation.

Author Manuscript Author Manuscript Author Manuscript Author Manuscript

Several brain insults, including hypoxia, seizures, trauma, and tumor invasion, can cause neuronal swelling (Glykys et al., 2017). Multiple pathways have been proposed to be involved in water movement during neuronal swelling. Notably, neurons lack aquaporins which allow free water movement in other cell types, such as astrocytes (Andrew et al., 2007). Although water can pass through lipid membranes, the inherent water permeability of the plasma membrane is low (2–50 10^{-4} cm/s), and it is influenced by the cholesterol composition (Fettiplace and Haydon, 1980; Haines, 1994; Tong et al., 2012). For the membranes of neurons, in particular, the water permeability is estimated to be ~4.69 10^{-3} cm/s (Boss et al., 2013) when water-permissible transporters are included in the calculation. Erythrocytes have similar water permeability, yet it decreases by a factor of four when AQP1 channels are blocked (Boss et al., 2013). Thus, most neuronal water permeability is likely due to channels rather than the direct movement of water through the lipid bilayer.

Various pathways have been proposed and observed to account for the movement of water into and out of neurons, as neuronal size regulation is essential for their survival. Some of these pathways involve CCCs, VRACs, monocarboxylate transporters, potassium channels, Na^+/H^+ exchangers, voltage-gated chloride channels, SLC26A11, TRPV4 (Hellas and Andrew, 2021; Meyer et al., 2021; Pasantes-Morales, 2016; Rungta et al., 2015; Wilson and Mongin, 2018). Importantly, in neurons, the movement of ions is intimately linked to that of water. In our study, we focused on CCCs because they have been implicated in the movement of water in a variety of cell types, and NKCC1 is highly expressed early during the development of the neocortex (Dzhala et al., 2005; Plotkin et al., 1997; Wang et al., 2002). Also, we studied not only prolonged but also brief OGD because the latter is frequently encountered in neonatal hypoxic-ischemic encephalopathy due to early intervention with oxygenation and resuscitation maneuvers.

Our experiments in layer IV/V of the neonatal neocortex showed that OGD leads to neuronal swelling and Cl^- accumulation, which can be reversed after 10 min and is dependent on extracellular Cl^-. Our results regarding changes in $[Cl^-]_i$ during OGD are similar to findings previously reported for adult murine slices (Galeffi et al., 2004; Pond et al., 2006). Our results that neuronal swelling depends on extracellular Cl^- are consistent with observations by other researchers using different approaches to induce swelling (Rungta et al., 2015; Steffensen et al., 2015; Weilinger et al., 2022). Importantly, our methodological approach also allowed us to determine what proportion of neurons increased, decreased, or did not change in size during OGD. Our observation that some neurons were resistant to OGD-induced swelling in the neocortex, whereas others were vulnerable, suggests that the average increase in neuronal size might be much higher if all neurons swelled. However, we decided to use all neurons that we could follow, rather than only those that responded, to get a better view of the changes in neuronal size that occur during OGD. This revealed an interesting phenomenon during reperfusion: even when the mean neuronal area dropped to baseline after 15 min of reperfusion, a significant number of swollen neurons did not decrease their size. Although we did not measure the neuronal survival rate or the degree of neuronal damage, our results suggest that 10 min of OGD is sufficient to cause persistent swelling in some neurons. It is unclear why some neurons swell and not others. This could represent a heterogenous population of neurons, some of which are more susceptible than others, or that

Author Manuscript Author Manuscript Author Manuscript Author Manuscript

some neurons require a stronger insult. Addressing why some neurons swell and not others could lead to novel approaches to reverse neuronal swelling.

Our finding that blocking NKCC1 reduced neocortical neuronal swelling during the neonatal period is consistent with observations made in several other systems. These include neuronal cultures perfused with NMDA (Jourdain et al., 2011), in young rats in vitro, perfused with NMDA yet reported as not statistically significant (Rungta et al., 2015), and in adult mice in vivo after close-cortical impact (Sawant-Pokam et al., 2020). NKCC1 null mice subjected to focal cerebral ischemia were shown to have less gray matter damage than wild-type counterparts (Chen et al., 2005), but it is unclear whether the effect is on astrocytes or neurons. The fact that blocking NKCC1 decreased neuronal swelling during early OGD in our experiments without preventing it at a later time suggests that other transport pathways may also be involved. For example, when the neuronal membrane depolarizes, a sizeable electro-chemical gradient favors the movement of Cl^- into neurons through any available path, including the recently described voltage-gated chloride channel, SLC26A11, which drags water in (Rungta et al., 2015). The lack of an effect of bumetanide at later times suggests that water influx continues via other available pathways, impacted by ionic derrangments during prolonged OGD.

Our study shows that KCC2 is also involved in neuronal water movement during the neonatal period but to a lesser degree. First, enhancing KCC2 activity prevented Cl^- accumulation but not neuronal swelling during prolonged and brief OGD, yet the mean MaxArea difference was negative compared to the no-drug condition. Second, blocking KCC2 activity caused a significant increase in the proportional change in $[Cl^-]_{i,}$ but not in neuronal swelling during the late phase of OGD (20 min). Third, blocking KCC2 during the washout resulted in a delay in the return to baseline neuronal size. Most likely, neuronal Cl^- does not reach sufficiently prolonged and high concentrations during brief OGD to reverse the NKCC1 activity (Brumback and Staley, 2008; DeFazio et al., 2000), so we postulate that KCC2 must do more work pumping Cl^- and water in this condition. When we blocked NKCC1 and KCC2 simultaneously, neuronal swelling at OGD-10′ still occurred, suggesting that water and Cl^- entered through other pathways. Similarly, our finding that blocking both transporters resulted in worse neuronal swelling at OGD-20′ and a faster increase in $[Cl^-]_i$ suggests that these transporters were actively working to pump water out during prolonged OGD. Therefore, NKCC1 and KCC2 are involved in water movement in neurons during early cortical development, but other water pathways are also present.

Our furosemide results suggest that water enters neurons through pathways other than CCCs. Furosemide prevented neuronal swelling and Cl^- accumulation during prolonged hypoxia to a higher degree than the impact of blocking NKCC1 and KCC2 simultaneously (with bumetanide plus VU0463271). These findings are consistent with previous observations on the outward movement of water through pathways besides CCCs, with neurons shrinking when the extracellular osmolarity was increased and when NKCC1 and KCC2 were blocked (Glykys et al., 2019; Glykys et al., 2014). Since furosemide blocks several transporters and enzymes, it is difficult to isolate its anti-swelling mechanism. When used in the micromolar range, as in our studies, furosemide has been reported to block $GABA_A$Rs, carbonic anhydrase, and Na^+-independent $Cl^-/HCO3^-$ exchanger (Halligan et

Author Manuscript Author Manuscript Author Manuscript Author Manuscript

al., 1991; Navon et al., 1975; Wafford et al., 1996). It could also block other undescribed pathways as well, as higher doses can even block NMDA currents (Lerma and Martin del Rio, 1992). Nevertheless, our results are consistent with evidence that furosemide prevents brain swelling in stroke models (Toung et al., 2002) and dendritic beading during spreading depolarization (Steffensen et al., 2015).

To conclude, our results shed light on the dynamics of neuronal swelling during brief and prolonged hypoxia in brain slices from the neocortex of neonatal mice. We found that blocking NKCC1 with bumetanide prevents early neuronal edema, while furosemide prevented swelling during early and prolonged hypoxia by blocking water import mechanisms besides those involving NKCC1 and KCC2. Thus, bumetanide and furosemide may be potential candidates for alleviating neuronal edema and mitigating brain damage due to hypoxia in neonates.

Supplementary Material

Refer to Web version on PubMed Central for supplementary material.

Acknowledgments

JG was funded by NIH/NINDS R01NS115800 and the Iowa Neuroscience Institute. YT was supported by a post-doctoral research fellowship from the American Epilepsy Society. Graphical abstract created with BioRender.

Data availability

Data will be made available on request.

References

Andrew RD, et al. , 2007. Physiological evidence that pyramidal neurons lack functional water channels. Cereb. Cortex 17, 787–802. 10.1093/cercor/bhk032. [PubMed: 16723408]

Azzopardi D, et al. , 2014. Effects of hypothermia for perinatal asphyxia on childhood outcomes. N. Engl. J. Med 371, 140–149. 10.1056/NEJMoa1315788. [PubMed: 25006720]

Berglund K, et al. , 2008. Imaging synaptic inhibition throughout the brain via genetically targeted Clomeleon. Brain Cell. Biol 36, 101–118. 10.1007/s11068-008-9031-x. [PubMed: 18850274]

Blauwblomme T, et al. , 2018. Transient ischemia facilitates neuronal chloride accumulation and severity of seizures. Ann. Clin. Transl. Neurol 5, 1048–1061. 10.1002/acn3.617. [PubMed: 30250862]

Boss D, et al. , 2013. Measurement of absolute cell volume, osmotic membrane water permeability, and refractive index of transmembrane water and solute flux by digital holographic microscopy. J. Biomed. Opt 18, 036007 10.1117/1.JBO.18.3.036007. [PubMed: 23487181]

Brumback AC, Staley KJ, 2008. Thermodynamic regulation of NKCC1-mediated clcotransport underlies plasticity of GABA(A) signaling in neonatal neurons. J. Neurosci 28, 1301–1312. 10.1523/JNEUROSCI.3378-07.2008. [PubMed: 18256250]

Chen H, et al. , 2005. Na(+)-dependent chloride transporter (NKCC1)-null mice exhibit less gray and white matter damage after focal cerebral ischemia. J. Cereb. Blood Flow Metab 25, 54–66. 10.1038/sj.jcbfm.9600006. [PubMed: 15678112]

Cooper DJ, et al. , 2011. Decompressive craniectomy in diffuse traumatic brain injury. N. Engl. J. Med 364, 1493–1502. 10.1056/NEJMoa1102077. [PubMed: 21434843]

Author Manuscript Author Manuscript Author Manuscript Author Manuscript

DeFazio RA, et al. , 2000. Potassium-coupled chloride cotransport controls intracellular chloride in rat neocortical pyramidal neurons. J. Neurosci 20, 8069–8076. 10.1523/jneurosci.20-21-08069.2000. [PubMed: 11050128]

Delpire E, Staley KJ, 2014. Novel determinants of the neuronal Cl(−) concentration. J. Physiol 592, 4099–4114. 10.1113/jphysiol.2014.275529. [PubMed: 25107928]

Doyon N, et al. , 2016. Chloride regulation: a dynamic equilibrium crucial for synaptic inhibition. Neuron 89, 1157–1172. 10.1016/j.neuron.2016.02.030. [PubMed: 26985723]

Duebel J, et al. , 2006. Two-photon imaging reveals somatodendritic chloride gradient in retinal ON-type bipolar cells expressing the biosensor Clomeleon. Neuron 49, 81–94. 10.1016/j.neuron.2005.10.035. [PubMed: 16387641]

Dusterwald KM, et al. , 2018. Biophysical models reveal the relative importance of transporter proteins and impermeant anions in chloride homeostasis. Elife 7 10.7554/eLife.39575.

Dzhala VI, Staley KJ, 2021. KCC2 chloride transport contributes to the termination of ictal epileptiform activity. eNeuro 8 10.1523/ENEURO.0208-20.2020.

Dzhala VI, et al. , 2005. NKCC1 transporter facilitates seizures in the developing brain. Nat. Med 11, 1205–1213. 10.1038/nm1301. [PubMed: 16227993]

Ebihara S, et al. , 1995. Gramicidin-perforated patch recording: GABA response in mammalian neurones with intact intracellular chloride. J. Physiol 484 (Pt 1), 77–86. 10.1113/jphysiol.1995.sp020649. [PubMed: 7541464]

Egawa K, et al. , 2013. Cl(−) homeodynamics in gap junction-coupled astrocytic networks on activation of GABAergic synapses. J. Physiol 591, 3901–3917. 10.1113/jphysiol.2013.257162. [PubMed: 23732644]

Fettiplace R, Haydon DA, 1980. Water permeability of lipid membranes. Physiol. Rev 60, 510–550. 10.1152/physrev.1980.60.2.510. [PubMed: 6992166]

Gagnon M, et al. , 2013. Chloride extrusion enhancers as novel therapeutics for neurological diseases. Nat. Med 19, 1524–1528. 10.1038/nm.3356. [PubMed: 24097188]

Galanopoulou AS, 2007. Developmental patterns in the regulation of chloride homeostasis and GABA(A) receptor signaling by seizures. Epilepsia 48 (Suppl. 5), 14–18. 10.1111/j.1528-1167.2007.01284.x.

Galeffi F, et al. , 2004. Changes in intracellular chloride after oxygen-glucose deprivation of the adult hippocampal slice: effect of diazepam. J. Neurosci 24, 4478–4488. 10.1523/JNEUROSCI.0755-04.2004. [PubMed: 15128862]

Gluckman PD, et al. , 2005. Selective head cooling with mild systemic hypothermia after neonatal encephalopathy: multicentre randomised trial. Lancet 365, 663–670. 10.1016/S0140-6736(05)17946-X. [PubMed: 15721471]

Glykys J, et al. , 2009. Differences in cortical versus subcortical GABAergic signaling: a candidate mechanism of electroclinical uncoupling of neonatal seizures. Neuron 63, 657–672. 10.1016/j.neuron.2009.08.022. [PubMed: 19755108]

Glykys J, et al. , 2014. Local impermeant anions establish the neuronal chloride concentration. Science 343, 670–675. 10.1126/science.1245423. [PubMed: 24503855]

Glykys J, et al. , 2017. Chloride dysregulation, seizures, and cerebral edema: a relationship with therapeutic potential. Trends Neurosci 40, 276–294. 10.1016/j.tins.2017.03.006. [PubMed: 28431741]

Glykys J, et al. , 2019. Mannitol decreases neocortical epileptiform activity during early brain development via cotransport of chloride and water. Neurobiol. Dis 125, 163–175. 10.1016/j.nbd.2019.01.024. [PubMed: 30711483]

Haines TH, 1994. Water transport across biological membranes. FEBS Lett 346, 115–122. 10.1016/0014-5793(94)00470-6. [PubMed: 8206149]

Halligan RD, et al. , 1991. Na(+)-independent Cl(−)-HCO3- exchange in sarcolemmal vesicles from vascular smooth muscle. Am. J. Phys 260, C347–C354. 10.1152/ajpcell.1991.260.2.C347.

Halstead MR, Geocadin RG, 2019. The medical management of cerebral edema: past, present, and future therapies. Neurotherapeutics 16, 1133–1148. 10.1007/s13311-019-00779-4. [PubMed: 31512062]

Author Manuscript Author Manuscript Author Manuscript Author Manuscript

Hamann S, et al. , 2010. Cotransport of water by the Na+-K+−2Cl(−) cotransporter NKCC1 in mammalian epithelial cells. J. Physiol 588, 4089–4101. 10.1113/jphysiol.2010.194738. [PubMed: 20819947]

Heathcote AC, et al. , 2018. Timing and documentation of key events in neonatal resuscitation. Eur. J. Pediatr 177, 1053–1056. 10.1007/s00431-018-3160-8. [PubMed: 29713811]

Hellas JA, Andrew RD, 2021. Neuronal swelling: a non-osmotic consequence of spreading depolarization. Neurocrit. Care 10.1007/s12028-021-01326-w.

Hoffmann EK, et al. , 2009. Physiology of cell volume regulation in vertebrates. Physiol. Rev 89, 193–277. 10.1152/physrev.00037.2007. [PubMed: 19126758]

Hutchinson PJ, et al. , 2016. Trial of decompressive craniectomy for traumatic intracranial hypertension. N. Engl. J. Med 375, 1119–1130. 10.1056/NEJMoa1605215. [PubMed: 27602507]

Jourdain P, et al. , 2011. Determination of transmembrane water fluxes in neurons elicited by glutamate ionotropic receptors and by the cotransporters KCC2 and NKCC1: a digital holographic microscopy study. J. Neurosci 31, 11846–11854. 10.1523/JNEUROSCI.0286-11.2011. [PubMed: 21849545]

Kahle KT, et al. , 2015. K-Cl cotransporters, cell volume homeostasis, and neurological disease. Trends Mol. Med 21, 513–523. 10.1016/j.molmed.2015.05.008. [PubMed: 26142773]

Kolias AG, et al. , 2022. Evaluation of outcomes among patients with traumatic intracranial hypertension treated with decompressive craniectomy vs standard medical care at 24 months: a secondary analysis of the RESCUEicp randomized clinical trial. JAMA Neurol 79, 664–671. 10.1001/jamaneurol.2022.1070. [PubMed: 35666526]

Kuner T, Augustine GJ, 2000. A genetically encoded ratiometric indicator for chloride: capturing chloride transients in cultured hippocampal neurons. Neuron 27, 447–459. 10.1016/s0896-6273(00)00056-8. [PubMed: 11055428]

Lerma J, Martin del Rio R, 1992. Chloride transport blockers prevent N-methyl-D-aspartate receptor-channel complex activation. Mol. Pharmacol 41, 217–222. [PubMed: 1371581]

Meyer J, et al. , 2021. Rapid fluorescence lifetime imaging reveals that TRPV4 channels promote dysregulation of neuronal Na(+) in ischemia. J. Neurosci 10.1523/JNEUROSCI.0819-21.2021.

Murguia-Castillo J, et al. , 2013. NKCC1 and KCC2 protein expression is sexually dimorphic in the hippocampus and entorhinal cortex of neonatal rats. Neurosci. Lett 552, 52–57. 10.1016/j.neulet.2013.07.038. [PubMed: 23932891]

Navon G, et al. , 1975. Application of the carbonic anhydrase inhibitory effect of furosemide to the study of furosemide release from two of its diuretic derivatives. J. Med. Chem 18, 1152–1154. 10.1021/jm00245a024. [PubMed: 1177262]

Obeidat AS, et al. , 2000. Glutamate does not mediate acute neuronal damage after spreading depression induced by O2/glucose deprivation in the hippocampal slice. J. Cereb. Blood Flow Metab 20, 412–422. 10.1097/00004647-200002000-00024. [PubMed: 10698080]

Orbach SA, et al. , 2014. Lower incidence of seizure among neonates treated with therapeutic hypothermia. J. Child Neurol 29, 1502–1507. 10.1177/0883073813507978. [PubMed: 24334344]

Pasantes-Morales H, 2016. Channels and volume changes in the life and death of the cell. Mol. Pharmacol 90, 358–370. 10.1124/mol.116.104158. [PubMed: 27358231]

Plotkin MD, et al. , 1997. Expression of the Na-K-2Cl cotransporter is developmentally regulated in post-natal rat brains: a possible mechanism underlying GABA's excitatory role in immature brain. J. Neurobiol 33, 781–795. 10.1002/(sici)1097-4695(19971120)33:6<781::Aid-neu6>3.0.Co;2-5. [PubMed: 9369151]

Pond BB, et al. , 2006. The chloride transporter Na(+)-K(+)-Cl- cotransporter isoform-1 contributes to intracellular chloride increases after in vitro ischemia. J. Neurosci 26, 1396–1406. 10.1523/JNEUROSCI.1421-05.2006. [PubMed: 16452663]

Portioli C, et al. , 2021. Cation-coupled chloride cotransporters: chemical insights and disease implications. Trends Chem 3, 832–849. 10.1016/j.trechm.2021.05.004. [PubMed: 34604727]

Povysheva N, et al. , 2019. Oxygen-glucose deprivation differentially affects neocortical pyramidal neurons and Parvalbumin-positive interneurons. Neuroscience 412, 72–82. 10.1016/j.neuroscience.2019.05.042. [PubMed: 31152933]

Author Manuscript Author Manuscript Author Manuscript Author Manuscript

Rahmati N, et al. , 2021. Unique actions of GABA arising from cytoplasmic chloride microdomains. J. Neurosci 41, 4957–4975. 10.1523/JNEUROSCI.3175-20.2021. [PubMed: 33903223]

Raimondo JV, et al. , 2012. Genetically encoded proton sensors reveal activity-dependent pH changes in neurons. Front. Mol. Neurosci 5, 68. 10.3389/fnmol.2012.00068. [PubMed: 22666186]

Risher WC, et al. , 2009. Real-time passive volume responses of astrocytes to acute osmotic and ischemic stress in cortical slices and in vivo revealed by two-photon microscopy. Glia 57, 207–221. 10.1002/glia.20747. [PubMed: 18720409]

Rungta RL, et al. , 2015. The cellular mechanisms of neuronal swelling underlying cytotoxic edema. Cell 161, 610–621. 10.1016/j.cell.2015.03.029. [PubMed: 25910210]

Saw CL, et al. , 2019. Current practice of therapeutic hypothermia for mild hypoxic ischemic encephalopathy. J. Child Neurol 34, 402–409. 10.1177/0883073819828625. [PubMed: 30898007]

Sawant-Pokam PA, et al. , 2020. Preventing neuronal edema increases network excitability after traumatic brain injury. J. Clin. Invest 130, 6005–6020. 10.1172/JCI134793. [PubMed: 33044227]

Sekhon MS, et al. , 2017. Clinical pathophysiology of hypoxic ischemic brain injury after cardiac arrest: a “two-hit” model. Crit. Care 21, 90. 10.1186/s13054-017-1670-9. [PubMed: 28403909]

Steffensen AB, et al. , 2015. Chloride cotransporters as a molecular mechanism underlying spreading depolarization-induced dendritic beading. J. Neurosci 35, 12172–12187. 10.1523/JNEUROSCI.0400-15.2015. [PubMed: 26338328]

Steffensen AB, et al. , 2018. Cotransporter-mediated water transport underlying cerebrospinal fluid formation. Nat. Commun 9, 2167. 10.1038/s41467-018-04677-9. [PubMed: 29867199]

Su G, et al. , 2002. Contribution of Na(+)-K(+)-Cl(−) cotransporter to high-[K(+)](o)-induced swelling and EAA release in astrocytes. Am. J. Phys. Cell Physiol 282, C1136–C1146. 10.1152/ajpcell.00478.2001.

Sulis Sato S, et al. , 2017. Simultaneous two-photon imaging of intracellular chloride concentration and pH in mouse pyramidal neurons in vivo. Proc. Natl. Acad. Sci. U. S. A 114, E8770–E8779. 10.1073/pnas.1702861114. [PubMed: 28973889]

Tong J, et al. , 2012. Water permeability of aquaporin-4 channel depends on bilayer composition, thickness, and elasticity. Biophys. J 103, 1899–1908. 10.1016/j.bpj.2012.09.025. [PubMed: 23199918]

Tong L, et al. , 2021. ANMAF: an automated neuronal morphology analysis framework using convolutional neural networks. Sci. Rep 11, 8179. 10.1038/s41598-021-87471-w. [PubMed: 33854113]

Toung TJ, et al. , 2002. Global brain water increases after experimental focal cerebral ischemia: effect of hypertonic saline. Crit. Care Med 30, 644–649. 10.1097/00003246-200203000-00025. [PubMed: 11990928]

Wafford KA, et al. , 1996. Functional characterization of human gamma-aminobutyric acidA receptors containing the alpha 4 subunit. Mol. Pharmacol 50, 670–678. [PubMed: 8794909]

Wang C, et al. , 2002. Developmental changes in KCC1, KCC2, and NKCC1 mRNA expressions in the rat brain. Dev. Brain Res 139, 59–66. 10.1016/s0165-3806(02)00536-9. [PubMed: 12414094]

Wang G, et al. , 2014. Bumetanide protects focal cerebral ischemia-reperfusion injury in rat. Int. J. Clin. Exp. Pathol 7, 1487–1494. [PubMed: 24817944]

Weilinger NL, et al. , 2022. KCC2 drives chloride microdomain formation in dendritic blebbing. Cell Rep 41, 111556 10.1016/j.celrep.2022.111556. [PubMed: 36288701]

Wilson CS, Mongin AA, 2018. Cell volume control in healthy brain and neuropathologies. Curr. Top. Membr 81, 385–455. 10.1016/bs.ctm.2018.07.006. [PubMed: 30243438]

Yamamoto C, Kawai N, 1968. Generation of the seizure discharge in thin sections from the guinea pig brain in chloride-free medium in vitro. Jpn J. Physiol 18, 620–631. 10.2170/jjphysiol.18.620. [PubMed: 5304232]

Yan Y, et al. , 2001. Na+-K+-cl- cotransporter in rat focal cerebral ischemia. J. Cereb. Blood Flow Metab 21, 711–721. 10.1097/00004647-200106000-00009. [PubMed: 11488540]

Yan Y, et al. , 2003. Inhibition of Na+–K+–cl cotransporter during focal cerebral ischemia decreases edema and neuronal damage. Brain Res 961, 22–31. 10.1016/s0006-8993(02)03832-5. [PubMed: 12535773]

Author Manuscript Author Manuscript Author Manuscript Author Manuscript

Zeuthen T, 1994. Cotransport of K+, Cl- and H2O by membrane proteins from choroid plexus epithelium of Necturus maculosus. J. Physiol 478 (Pt 2), 203–219. 10.1113/jphysiol.1994.sp020243. [PubMed: 7965842]

Zeuthen T, 2010. Water-transporting proteins. J. Membr. Biol 234, 57–73. 10.1007/s00232-009-9216-y. [PubMed: 20091162]

Zeuthen T, Macaulay N, 2012. Cotransport of water by Na(+)-K(+)-2Cl(−) cotransporters expressed in Xenopus oocytes: NKCC1 versus NKCC2. J. Physiol 590, 1139–1154. 10.1113/jphysiol.2011.226316. [PubMed: 22250214]

Zhang S, et al. , 2021. The structural basis of function and regulation of neuronal cotransporters NKCC1 and KCC2. Commun. Biol 4, 226. 10.1038/s42003-021-01750-w. [PubMed: 33597714]

Author Manuscript Author Manuscript Author Manuscript Author Manuscript

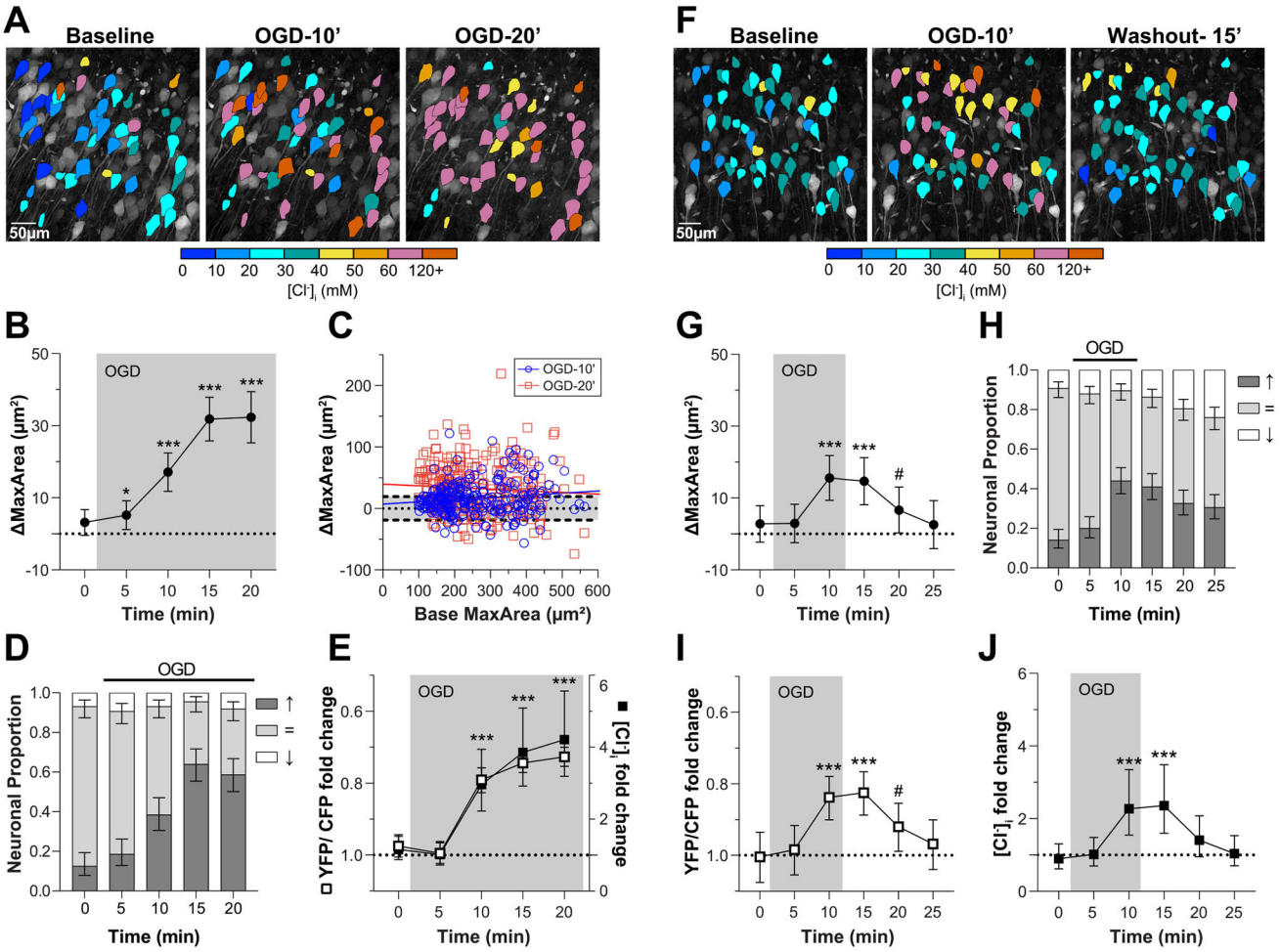

Fig. 1.

OGD causes neonatal neocortical neurons to swell and accumulate Cl^-

A) $[Cl^-]_i$ pseudo-colored on a two-photon stack image (YFP, maximal projection) of a P12 neocortical slice (layer IV/V) expressing Clomeleon at baseline (aCSF-0′), after 10-min OGD (OGD-10′), and after 20-min OGD (OGD-20′). **B)** Change in neuronal MaxArea from baseline during prolonged OGD. N = 247 paired neurons,10 slices, 3 mice. **C**) Correlation between baseline and change in MaxArea at OGD-10′ and OGD-20′. Gray box between dashed lines: 1 SD (19.3 µm^2). OGD-10′: m = 0.035 [0.004, 0.066]: R^2 = 0.02, p = 0.022. OGD-20′: m = 0.027 [0.074, 0.020]: R^2 = 0.005, p = 0.255. **D)** Proportion of neurons whose MaxArea changed by >19.3 µm^2 during OGD. **E)** Fold change in YFP/CFP (left y-axis) and $[Cl^-]_i$ (right-axis) during prolonged OGD. **F)** Same as A but including 15-min reperfusion (washout-15′) in place of OGD-20′. **G)** Change in neuronal MaxArea during brief OGD experiments. n = 425 paired neurons, 10 slices, 3 mice. **H)** Proportion of neurons that changed >19.3 µm^2 during brief OGD experiments. **I)** Fold change in YFP/CFP during brief OGD. **J)** Fold change in $[Cl^-]_i$ during brief OGD. Gray box in each panel marks the period of OGD perfusion. Time 0 min represents the difference between two different aCSF time points. Values: mean ± 95% CI, except for $[Cl^-]_i$ and YFP/CFP, which are geometric

means ±95% CI. Linear mixed model analysis, #$p < 0.05$, *$p < 0.01$, **$p < 0.001$, ***$p < 0.0001$. OGD, oxygen-glucose deprivation.

Author Manuscript Author Manuscript Author Manuscript Author Manuscript

Author Manuscript Author Manuscript Author Manuscript Author Manuscript

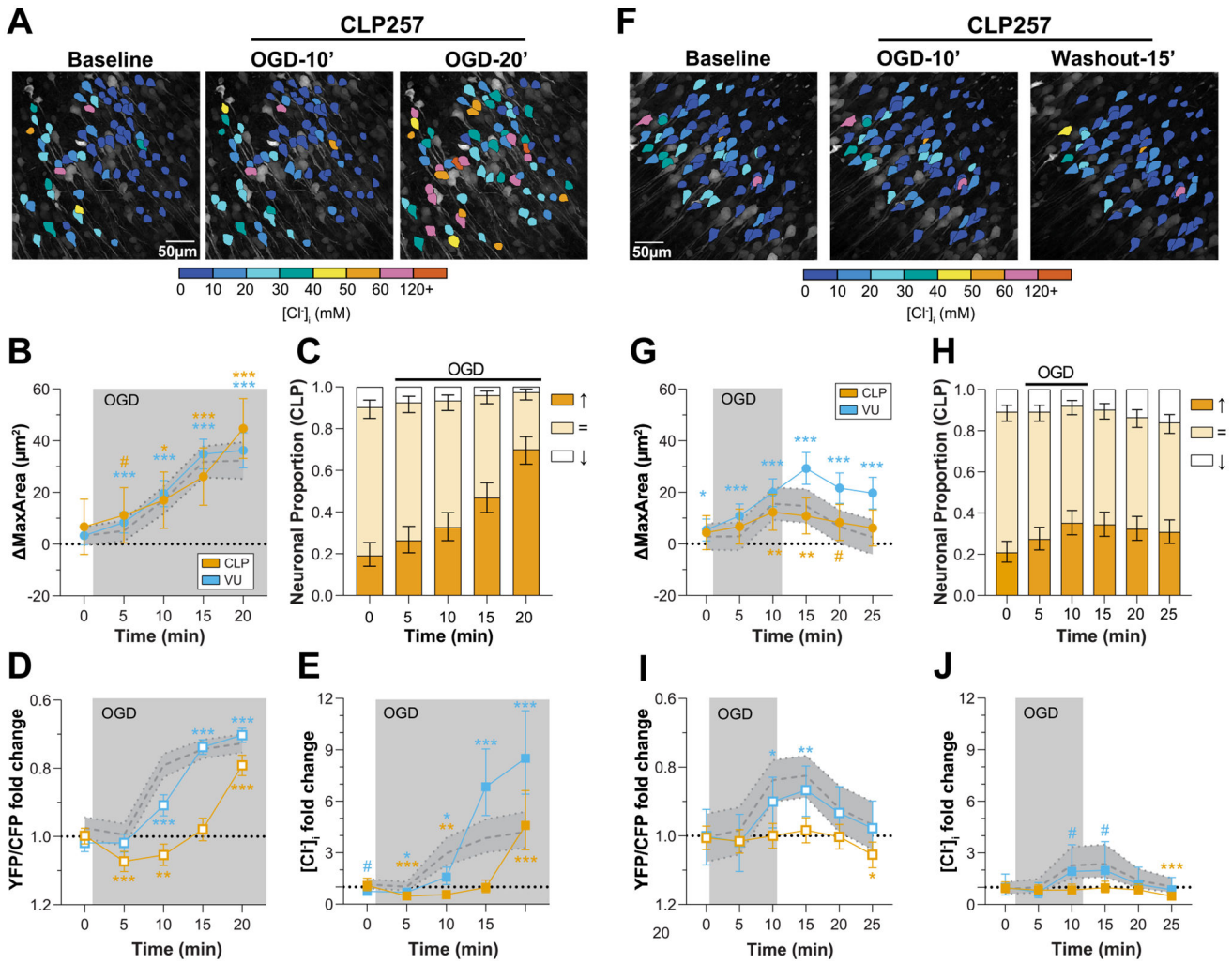

Fig. 2.

Enhancing KCC2 activity does not decrease OGD-induced neuronal swelling but prevents Cl^- accumulation in the neonatal neocortex.

A) $[Cl^-]_i$ pseudo-colored on a two-photon stack image (YFP, maximal projection) of a P10 neocortical slice (layer IV/V) expressing Clomeleon at baseline (aCSF-0′) and perfused with the KCC2 agonist CLP257 (10 µM) during OGD-10′ and OGD-20′. **B)** Change in neuronal MaxArea during prolonged OGD compared to baseline in the presence of CLP257 (baseline 232 μm^2 [198, 266]) or VU0463271 (baseline 251 μm^2 [228, 274]). Dashed line: prolonged OGD with no drug, mean ± 95% CI. **C)** Proportion of neurons whose MaxArea changed by >19.3 μm^2 during OGD in CLP257. **D)** Fold change in YFP/CFP at each timepoint during prolonged OGD in CLP257 or VU0463271. **E)** Fold change in $[Cl^-]_i$ during prolonged OGD in CLP257 (baseline 16.3 mM [6.82, 38.9]) or VU0463271 (baseline 12.8 mM [10.4, 15.8]). **F)** Same as A but including 15-min of reperfusion (washout-15′) in place of OGD-20′ under CLP257. **G)** Change in neuronal MaxArea during brief OGD experiments compared to baseline in the presence of CLP257 (baseline: 230 μm^2 [186, 275]) or VU0463271 (baseline size: 250 μm^2 [220, 281]). Dashed line: Brief OGD with no drug, mean ± 95% CI. **H)** Proportion of neurons whose MaxArea changed by >19.3 μm^2 during brief OGD in

Author Manuscript Author Manuscript Author Manuscript Author Manuscript

CLP257. **I)** Fold change in YFP/CFP during brief OGD in CLP257 or VU0463271. **J)** Fold change in $[Cl^-]_i$ during brief OGD in CLP257 (baseline 10.6 mM [6.21, 18]) or VU0463271 (baseline: 12.6 mM [7.09, 22.6]). Gray box in each panel marks periods of OGD perfusion in the presence of CLP257 or VU0463271. Time 0 min represents the difference between aCSF and drug perfusion. Values: mean ± 95% CI, except for $[Cl]_i$ and YFP/CFP, which are geometric means ±95% CI. Linear mixed model analysis, #$p < 0.05$, *$p < 0.01$, **$p < 0.001$, ***$p < 0.0001$. OGD, oxygen-glucose deprivation; CLP, CLP257; VU, VU0463271.

Author Manuscript Author Manuscript Author Manuscript Author Manuscript

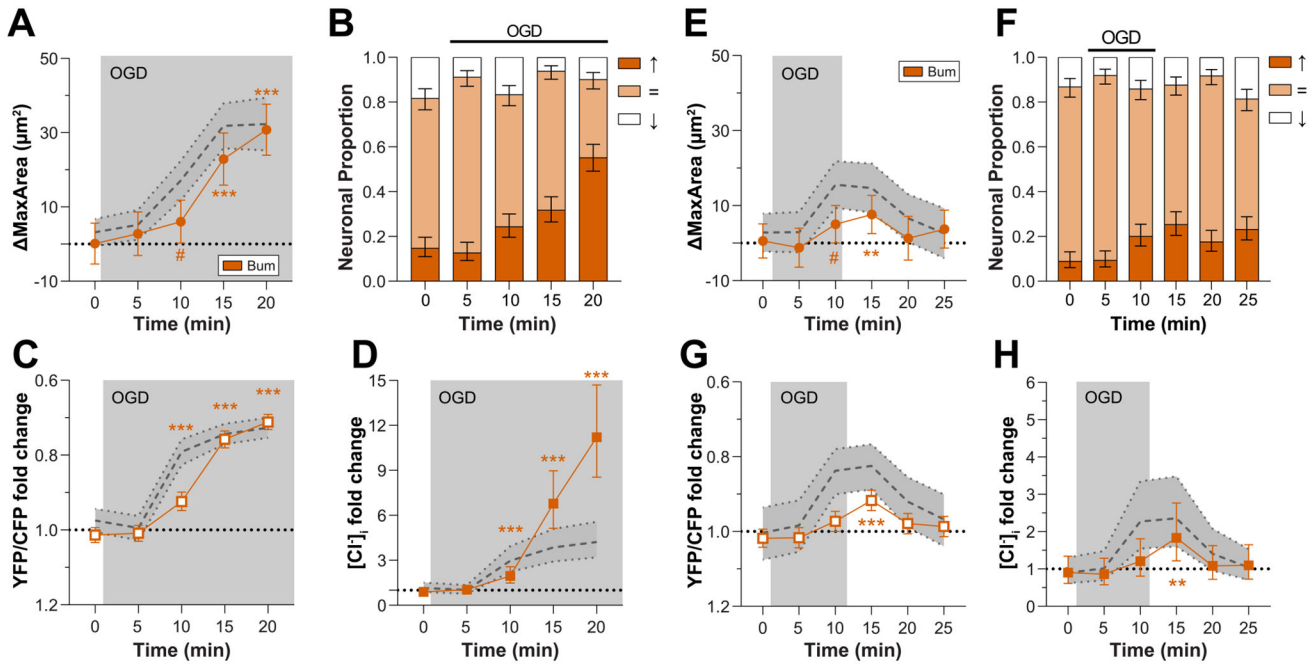

Fig. 3.

Blocking NKCC1 decreases neuronal swelling and Cl^- accumulation during early OGD in the neonatal neocortex.

A) Change in neuronal MaxArea during prolonged OGD following treatment with bumetanide (10 μM). Baseline: 248 μm^2 [234, 262], n = 487 paired neurons, 18 slices, 6 mice. Dashed line: prolonged OGD with no drug, mean ± 95% CI. **B)** Proportion of neurons whose MaxArea changed >19.3 μm^2 during OGD in the presence of bumetanide. **C)** Fold change in YFP/CFP during prolonged OGD in the presence of bumetanide. **D)** Fold change in $[Cl^-]_i$ at each timepoint during prolonged OGD in the presence of bumetanide (baseline: 6.53 mM [3.96, 10.7]). **E)** Change in neuronal MaxArea during brief OGD in the presence of bumetanide. Baseline 239 μm^2 [214, 265], n = 518 paired neurons, 16 slices, 6 mice. Dashed line: Brief OGD with no drug, mean ± 95% CI. **F)** Proportion of neurons whose MaxArea changed >19.3 μm^2 during OGD in the presence of bumetanide. **G)** Fold change in YFP/CFP during brief OGD in the presence of bumetanide. **H)** Fold change in $[Cl^-]_i$ during brief OGD in the presence of bumetanide (baseline: 8.62 mM [4.65, 16]). Gray box in each panel marks the period of OGD perfusion. Time 0 min represents the difference between aCSF and drug perfusion.Values: mean ± 95% CI, except for $[Cl^-]_i$ and YFP/CFP, which are geometric means ±95% CI. Linear mixed model analysis, #$p < 0.05$, *$p < 0.01$, **$p < 0.001$, ***$p < 0.0001$. OGD, oxygen-glucose deprivation.

Author Manuscript Author Manuscript Author Manuscript Author Manuscript

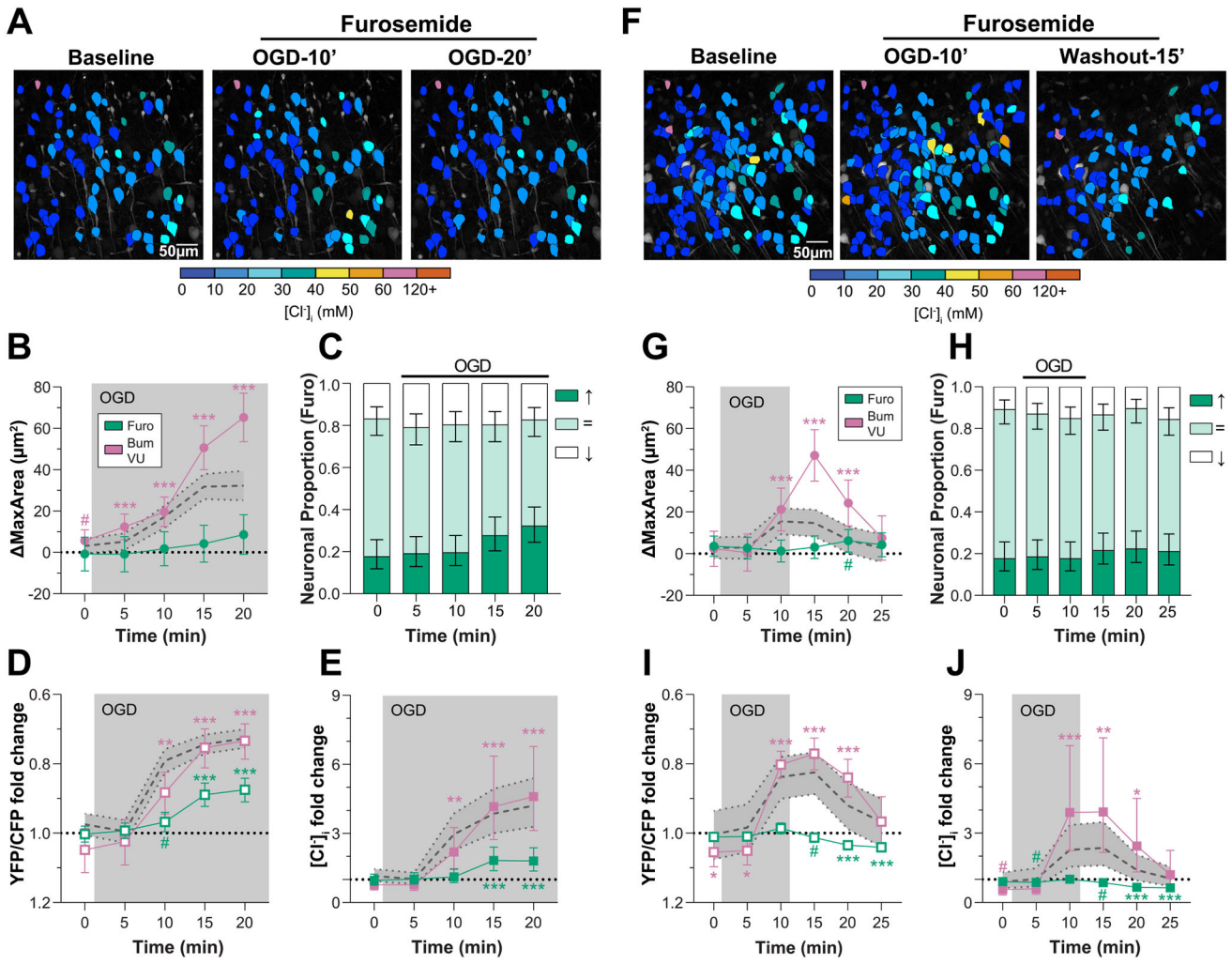

Fig. 4.

Furosemide, but not the simultaneous blocking of NKCC1 and KCC2, reduces neuronal swelling and Cl^- accumulation during prolonged OGD in the neonatal neocortex.

A) $[Cl^-]_i$ pseudo-colored on a two-photon stack image (YFP, maximal projection) of a P11 neocortical slice (layer IV/V) expressing Clomeleon at baseline (aCSF 0 min), OGD-10′, and OGD-20′ in furosemide (300 µM). **B)** Change in neuronal MaxArea during prolonged OGD compared to baseline in furosemide (baseline 229 μm^2 [208, 249]), or bumetanide + VU0463271 (baseline: 294 μm^2 [230, 358]). Dashed line: prolonged OGD with no drug, mean ± 95% CI. **C)** Proportion of neurons whose MaxArea changed by >19.3 μm^2 during OGD in furosemide. **D)** Fold change in YFP/CFP at each time point during prolonged OGD in furosemide or bumetanide + VU0463271. **E)** Fold change in $[Cl^-]_i$ during prolonged OGD in furosemide (baseline: 29.8 mM [18, 49]) or bumetanide + VU0463271 (baseline: 28 mM [20.3, 38.5]). **F)** Same as A but including 15-min reperfusion (washout-15′) in place of OGD-20′ in the presence of furosemide. **G)** Change in neuronal MaxArea during brief OGD in furosemide (baseline: 234 μm^2 [211, 256]) or bumetanide + VU0463271 (254 μm^2 [218, 290]). Dashed line: Brief OGD with no drug, mean ± 95% CI. **H)** Proportion of neurons whose MaxArea changed >19.3 μm^2 during brief OGD in furosemide. **I)** Fold change in

Author Manuscript Author Manuscript Author Manuscript Author Manuscript

YFP/CFP during brief OGD in furosemide or Bum+VU. **J)** Fold change in $[Cl^-]_i$ during brief OGD in furosemide (baseline 27.44 mM [17.7, 42.6]) or bumetanide + VU0463271 (baseline: 18.7 mM [7.71, 45.5]). Gray box in each panel marks the period of OGD perfusion. Time 0 min represents the difference between aCSF and drug perfusion.Values: mean ± 95% CI, except for $[Cl^-]_i$ and YFP/CFP, which are geometric means ±95% CI. Linear mixed model analysis, #$p < 0.05$, *$p < 0.01$, **$p < 0.001$, ***$p < 0.0001$. OGD, oxygen-glucose deprivation; Furo, furosemide.

Author Manuscript Author Manuscript Author Manuscript Author Manuscript

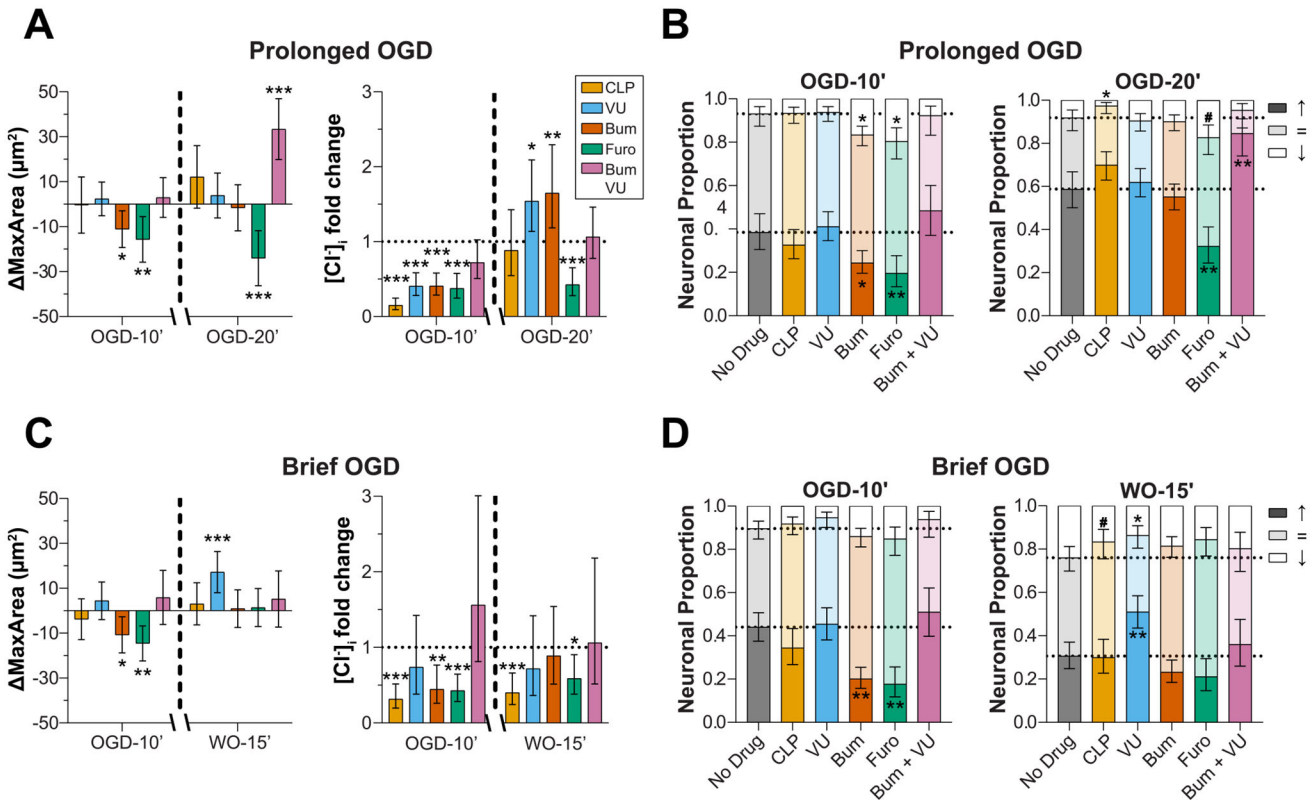

Fig. 5.

Comparison of drug effects on neuronal swelling and Cl^- accumulation during prolonged and brief OGD in the neonatal neocortex.

A) Change in neuronal MaxArea *(left)* and fold change in $[Cl^-]_i$ *(right)* during prolonged OGD for each group compared to no-drug condition (CLP257: 346 paired neurons, 6 slices, 3 mice; VU0463271 389 paired neurons, 8 slices, 4 mice; bumetanide 487 paired neurons, 18 slices, 6 mice; furosemide 220 paired neurons, 8 slices, 4 mice; bumetanide + VU0463271: 130 paired neurons, 6 slices, 3 mice; no-drug 247 paired neurons, 10 slices, 3 mice. **B)** Proportion of neurons whose area changed by >19.3 μm^2 during prolonged OGD (*left:* OGD-10′; *right*: OGD-20′). White: shrunken neurons, Black: swollen neurons. **C)** Same as A but for brief OGD experiments (CLP257: 495 paired neurons, 6 slices, 3 mice; VU0463271: 339 paired neurons, 8 slices, 4 mice; bumetanide 518 paired neurons, 16 slices, 6 mice; furosemide: 233 paired neurons, 8 slices, 4 mice; bumetanide + VU0463271: 147 paired neurons, 6 slices, 3 mice; no-drug: 425 paired neurons, 10 slices, 3 mice). **D)** Same as B but for brief OGD experiments. Values: mean ± 95% CI, except for $[Cl^-]_i$ and YFP/CFP ratio, which are geometric means ±95% CI. Linear mixed model analysis, #$p < 0.05$, *$p < 0.01$, **$p < 0.001$, ***$p < 0.0001$. OGD, oxygen-glucose deprivation; CLP, CLP257; VU, VU0463271; Bum, bumetanide; Furo, furosemide. The *p*-values were adjusted for multiple comparisons and the number of time points.